Measurements of two- and three-spin parameters at 6 GeV/c using a transversely polarized beam and target

A. Beretvas* and D. Miller
Northwestern University, Evanston, Illinois 60201

I. P. Auer, R. Giese, D. Hill, K. Nield, P. Rynes, B. Sandler,† Y. Watanabe,‡ and A. Yokosawa
Argonne National Laboratory, Argonne, Illinois 60439

(Received 25 August 1978)

Toward the goal of experimentally determining pp elastic scattering amplitudes at 6 GeV/c, we have measured a linear combination of triple-spin correlation parameters and also a linear combination of spin-transfer parameters over the $|t|$ range between 0.2 and 1.0 (GeV/c)^2. A horizontally polarized beam (S direction) was obtained by precessing the spin of the polarized beam from the Argonne Zero Gradient Synchrotron using a superconducting solenoid. The target protons were polarized vertically (N direction) and the polarization of the recoil protons was measured with a carbon polarimeter. The results are consistent with the amplitude corresponding to π exchange being almost real and positive.

I. INTRODUCTION

At low energies the proton-proton elastic scattering process has been successfully described by phase-shift analyses, which efficiently utilize rather limited types of experimental data, e.g., the differential cross section and polarization.[1] But, above P_{lab} of about 1 GeV/c, where the inelastic channels start taking a large part of the cross section, the analyses become increasingly difficult because of the large number of parameters involved.

In 1961, Schumacher and Bethe[2] pointed out that even at higher energy there are ways to reconstruct the scattering amplitudes in a limited $|t|$ range by measuring a certain set of observables, which are expressed in bilinear form in terms of five complex amplitudes. As the overall phase remains arbitrary, at least nine measurements are required to determine the amplitudes aside from discrete ambiguities, which can be removed by additional measurements. Realizing this experimentally, however, was thought to be almost impossible until recently because most of the measurements would require double or triple scattering and thus suffer from very poor statistics.

The situation was changed considerably by the successful acceleration of polarized-proton beams up to 12 GeV/c at Argonne National Laboratory, together with advances in polarized-target techniques. An extensive program is now in progress to determine proton-proton elastic scattering amplitudes beginning at 6 GeV/c over the $|t|$ range of 0.2 to 1.0 (GeV/c)^2. The experiment reported here is one in the program in which we simultaneously measured the triple-spin parameter H_{SNS} and as a by-product the spin-transfer parameter K_{SS}.

In Sec. II these parameters are defined and related to scattering amplitudes. Section III contains a description of the experimental apparatus, especially the carbon polarimeter, which is an essential new piece of the equipment. The data analysis and the results are given in Sec. IV, and the details of experimental biases are examined in the Appendix B. Our results will be combined with our later measurements to reconstruct the scattering amplitudes, as described earlier. However, we discuss the immediate results on the amplitudes constrained by these measurements in Sec. V.

II. EXPERIMENTAL OBSERVABLES

The experimental observables can be written as $I_n(B,T;S,R)$, where B, T, S, and R describe the spin state of the beam, target, forward scattered, and slow recoil protons, respectively; the number of elastic events I is expressed as

$$I=I_0[1+P_B I_n(B,0;0,0)+P_T I_n(0,T;0,0)+P_B P_T I_n(B,T;0,0)+\cdots],$$

where I_0 is the number of spin-averaged events. [Note that the notation $I_n(B,T;S,R)$ is equivalent to the notation $(B,T;S,\underrightarrow{R})$ used in our previous publications.] We define $\vec{N}$ as the normal to the scattering plane, $\vec{L}$ along the direction of motion of the proton being considered, and $\vec{S}=\vec{N}\times\vec{L}$, as shown in Fig. 1. For the target at rest, we use the same coordinate system as for the beam. If an initial particle is unpolarized or the polarization of a final-state particle is not analyzed, it is specified by 0. Thus, there are $4^4=256$ possible scattering observables, most of which are zero or redundant. We use short-hand notations for these observables:

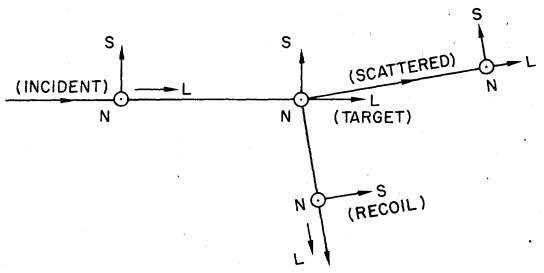

N: NORMAL TO THE SCATTERING PLANE
L: LONGITUDINAL DIRECTION
S = N x L IN THE SCATTERING PLANE

FIG. 1. The definition of spin directions $\vec{N}$, $\vec{L}$, and $\vec{S}$.

$P = I_n(N,0;0,0) = I_n(0,N;0,0)$, polarization parameter,

$C_{ij} = I_n(i,j;0,0)$, spin-spin correlation parameter,

$D_{ij} = I_n(0,i;0,j)$, depolarization parameter,

$K_{ij} = I_n(i,0;0,j)$, spin-transfer parameter,

and

$H_{ijk} = I_n(i,j;0,k)$, triple-spin correlation parameter.

Here, i, j, and k are either N, L, or S.

These observables can be described by a set of elastic scattering amplitudes. As a spin-$\frac{1}{2}$ particle is described by two complex amplitudes, there are $2^4 = 16$ complex amplitudes in general. The number of independent amplitudes is reduced to six by parity and time-reversal invariance, and then to five owing to identical-particle symmetry.

We use t-channel-exchange-helicity amplitudes, N_0, N_1, N_2, U_0, and U_2, where N (U) indicates natural- (unnatural-) parity exchange at asymptotic energy and the subscripts indicate the amount of helicity flip.[3] In terms of more familiar s-channel-helicity amplitudes $\phi_1 = \langle ++|++\rangle$, $\phi_2 = \langle --|++\rangle$, $\phi_3 = \langle +-|+-\rangle$, $\phi_4 = \langle +-|-+\rangle$, and $\phi_5 = \langle ++|+-\rangle$:

$$N_0 = \tfrac{1}{2}(\phi_1 + \phi_3), \quad N_1 = \phi_5, \quad N_2 = \tfrac{1}{2}(\phi_4 - \phi_2),$$

$$U_0 = \tfrac{1}{2}(\phi_1 - \phi_3), \quad U_2 = \tfrac{1}{2}(\phi_2 + \phi_4).$$

In Table I, the experimental observables are expressed in terms of these amplitudes.

A method of reconstructing the amplitudes, which is particularly suited for our experimental capabilities, has been proposed by Johnson, Miller, and Thomas.[4] Their choice of nine observables is $d\sigma_0$, P, C_{NN}, C_{SS}, C_{SL}, C_{LL}, K_{NN}, D_{NN}, and H_{SNS}.[5-11] They showed that these measurements give rise to threefold discrete ambiguities, two of which can be removed by the measurements of D_{LS} and H_{NSS}. The remaining ambiguity produces no notable distinction in terms of the amplitude results. Additional measurements, especially D_{SS} and H_{LSN}, help to reduce the overall uncertainties of amplitudes.

III. EXPERIMENTAL EQUIPMENT

The experimental layout is shown in Fig. 2. It consists of a polarized-proton target (PPT), an array of multiwire proportional chambers, and a set of trigger scintillation counters. The apparatus is similar to that described in an earlier publication,[9] which also contains details of the analysis procedure. An essential new piece of equipment in this experiment is a recoil polarimeter, which is described in detail later in this section.

A. Polarized-proton target (PPT)

The direction of the magnetic field and thus the polarization of the target was vertical; i.e., normal to the nominal scattering plane. The magnet provided a field of 2.5 T with a uniformity of better than 10^{-3} over the target region. The target was $2\times2\times8$-cm^3 ethylene glycol ($HOCH_2CH_2OH$) doped with $K_2Cr_2O_7$, and was maintained at 0.4 K by a ^{3}He refrigerator. Polarization was dynamically produced by microwave "spin pumping" and monitored by an NMR system. The NMR signals were analyzed continuously on-line by a PDP-11 computer. About 9% of the nucleons in the target were free protons and polarized to an average $P_T = 0.80$. The estimated number of free protons was 3.5×10^{-4}/mb. The target polarization was reversed every 2–3 h to provide matched running conditions.

B. Polarized-proton beam

The spin direction of the polarized beam from the Argonne Zero Gradient Synchrotron (ZGS) was rotated by a superconducting solenoid from the $\vec{N}$ to the $\vec{S}$ direction. The line-integral field required at $P = 6$ GeV/c is

$$\int \vec{B}\cdot d\vec{l} = \frac{\pi/2}{(e/pc)\frac{1}{2}g} = 11.2 \text{ T m},$$

where $\frac{1}{2}g = 2.79$. The beam polarization P_B was typically 0.7, and the spin direction was reversed at the ZGS source every spill. The beam intensity was about 5×10^5 protons/pulse and had a divergence of ±5 mrad.

The PPT magnetic field precessed the spin of the beam protons by 14.6° at the center of the target, giving the beam polarization a 25% L component.

TABLE I. Laboratory observables in terms of t-channel helicity amplitudes. The quantity $\Delta\sigma_L = \sigma_{\rightrightarrows}^{\text{tot}} - \sigma_{\rightleftarrows}^{\text{tot}}$ is the difference between total cross sections for parallel and antiparallel in longitudinal spin states. (θ_R is the laboratory recoil angle.)

Observables $(B,T;S,R)$	Exchange amplitudes
	Single scattering
σ^{tot}	$\propto \text{Im}N_0\|_{t=0}$
$\Delta\sigma_L^{\text{tot}}$	$\propto \text{Im}U_0\|_{t=0}$
$\Delta\sigma_T^{\text{tot}}$	$\propto \text{Im}U_2\|_{t=0} = -\text{Im}N_2\|_{t=0}$
$\sigma_0 = I_n(0,0;0,0)$	$\|N_0\|^2 + 2\|N_1\|^2 + \|N_2\|^2 + \|U_0\|^2 + \|U_2\|^2$
$P = I_n(0,N;0,0)$	$-2\,\text{Im}\{(N_0 - N_2)N_1^*\}/\sigma_0$ [also $I_n(N,0;0,0)$]
$C_{NN} = I_n(N,N;0,0)$	$2\,\text{Re}(U_0U_2^* - N_0N_2^* + \|N_1\|^2)/\sigma_0$
$C_{SS} = I_n(S,S;0,0)$	$2\,\text{Re}(N_0U_2^* - N_2U_0^*)/\sigma_0$
$C_{SL} = I_n(S,L;0,0)$	$2\,\text{Re}\{(U_0 + U_2)N_1^*\}/\sigma_0$
$C_{LL} = I_n(L,L;0,0)$	$-2\,\text{Re}(N_0U_0^* - N_2U_2^*)/\sigma_0$
	Double scattering
(1) K_{jk} measurement	
$K_{NN} = I_n(N,0;0,N)$	$-2\,\text{Re}(U_0U_2^* + N_0N_2^* - \|N_1\|^2)/\sigma_0$
$K_{SS} = I_n(S,0;0,S)$	$[-2\,\text{Re}\{(U_2 - U_0)N_1^*\}\sin\theta_R - 2\,\text{Re}(N_0U_2^* + N_2U_0^*)\cos\theta_R]/\sigma_0$
$K_{LS} = I_n(L,0;0,S)$	$\{-2\,\text{Re}(N_0U_0^* + N_2U_2^*)\sin\theta_R - 2\,\text{Re}[N_1^*(U_2 - U_0)]\cos\theta_R\}/\sigma_0$
(2) D_{jk} measurement	
$D_{NN} = I_n(0,N;0,N)$	$\{\|N_0\|^2 + 2\|N_1\|^2 + \|N_2\|^2 - \|U_0\|^2 - \|U_2\|^2\}/\sigma_0$
$D_{SS} = I_n(0,S;0,S)$	$[-2\,\text{Re}\{(N_0 + N_2)N_1^*\}\sin\theta_R - (\|N_0\|^2 - \|N_2\|^2 + \|U_2\|^2 - \|U_0\|^2)\cos\theta_R]/\sigma_0$
$D_{LS} = I_n(0,L;0,S)$	$[(\|N_0\|^2 - \|N_2\|^2 - \|U_2\|^2 + \|U_0\|^2)\sin\theta_R - 2\,\text{Re}\{(N_0 + N_2)N_1^*\}\cos\theta_R]/\sigma_0$
(3) Three-spin measurement	
$H_{SNS} = I_n(S,N;0,S)$	$[2\,\text{Im}(N_0U_2^* + N_2U_0^*)\sin\theta_R + 2\,\text{Im}\{(U_2 - U_0)N_1^*\}\cos\theta_R]/\sigma_0$
$H_{NSS} = I_n(N,S;0,S)$	$[-2\,\text{Im}(U_0U_2^* - N_0N_2^*)\sin\theta_R + 2\,\text{Im}\{(N_0 + N_2)N_1^*\}\cos\theta_R]/\sigma_0$
$H_{SSN} = I_n(S,S;0,N)$	$-2\,\text{Im}\{(U_2 + U_0)N_1^*\}/\sigma_0$
$H_{LSN} = I_n(L,S;0,N)$	$2\,\text{Im}(U_0N_0^* - U_2N_2^*)/\sigma_0$
$H_{NLS} = I_n(N,L;0,S)$	$[-2\,\text{Im}\{(N_0 + N_2)N_1^*\}\sin\theta_R + 2\,\text{Im}(U_0U_2^* + N_0N_2^*)\cos\theta_R]/\sigma_0$
$H_{SLN} = I_n(S,L;0,N)$	$-2\,\text{Im}(N_0U_2^* - N_2U_0^*)/\sigma_0$
	Simultaneous observables
H_{SNS}, $I_n(0,N;0,N)$, $I_n(S,0;0,S)$	
H_{NSS}, $I_n(0,S;0,S)$, $I_n(N,0;0,N)$	
H_{SSN}, $I_n(S,S;0,0)$, $I_n(0,S;0,S)$, $I_n(S,0;0,S)$	
H_{LSN}, $I_n(0,S;0,S)$, $I_n(L,0;0,S)$, $I_n(L,S;0,0)$	
H_{NLS}, $I_n(0,L;0,S)$, $I_n(N,0;0,N)$	
H_{SLN}, $I_n(S,L;0,0)$, $I_n(0,L;0,S)$, $I_n(S,0;0,S)$	

C. Event logic and detection equipment

The incident beam was defined by a triple coincidence of scintillation counters S_0, S_1, and S_2, vetoed by a hole counter BA1. The event trigger was defined by requiring an additional coincidence of at least one forward counter and one recoil counter together with no signals from anticounters

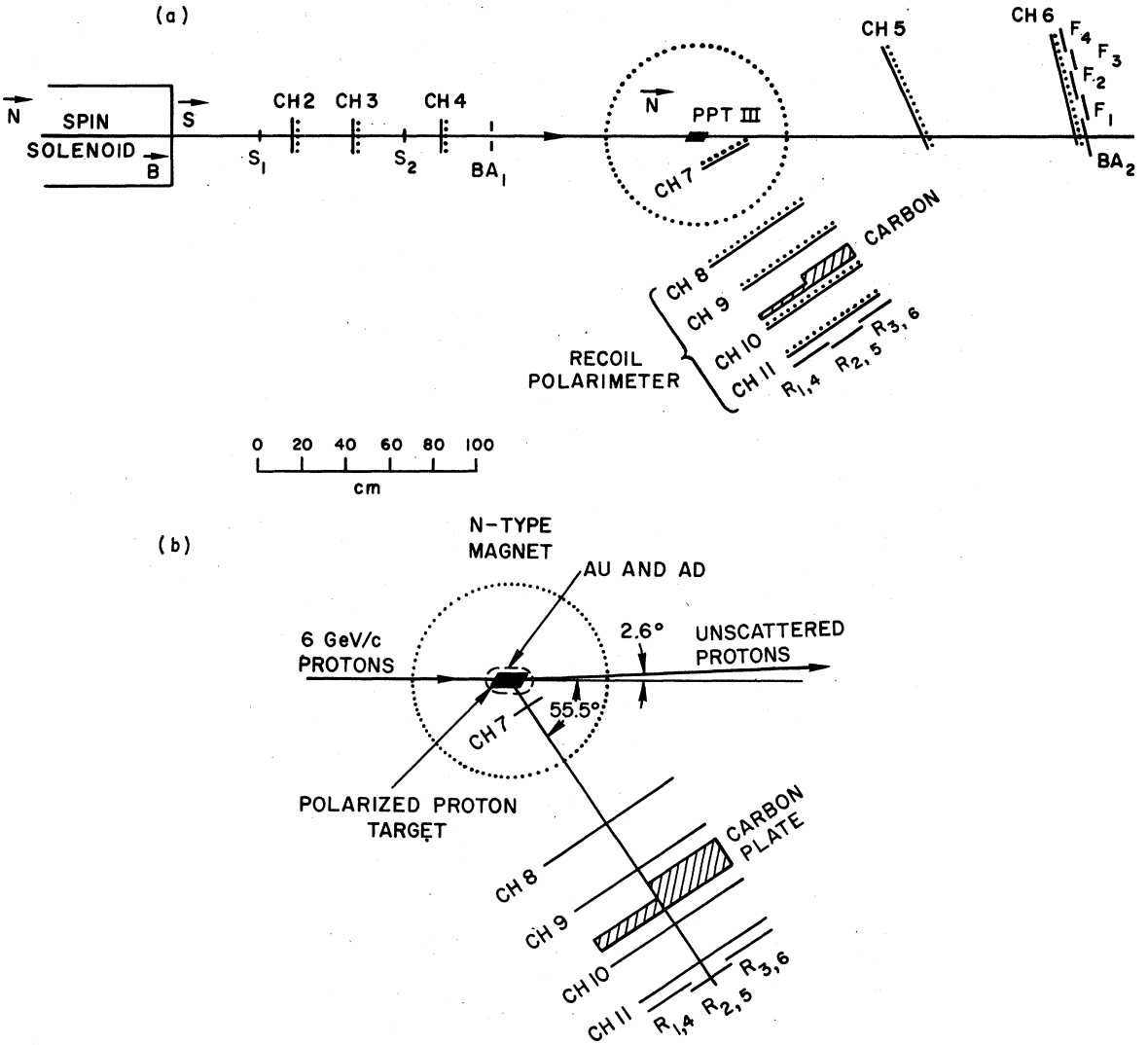

FIG. 2. (a) Schematic layout of the experimental apparatus. (b) The recoil polarimeter and typical trajectories of recoil protons at various t.

placed at the PPT magnet pole faces (AU and AD) and directly in the beam (BA2). Eleven multiwire proportional chambers (MWPC) recorded the tracks of the beam, forward, recoil, and scattered recoil protons in the carbon plate. The information of hits of MWPC's (CHI-11), hits of counters, and scalar values was read into an EMR 6050 computer and written on tape to be analyzed off-line.

D. Carbon polarimeter

The essential new piece of the apparatus was a carbon polarimeter which allowed the measurement of the recoil polarization in the $\hat{S}$ and $\hat{N}$ directions. Similar polarimeters have been used by other groups.[8,11] The polarimeter consisted of four MWPC's and a piece of carbon as shown in Fig. 2. The chambers all had 2-mm wire spacing; the first two had 256×128 wires and the last two had 256×256 wires. The thickness of the thin part of the carbon was $\frac{3}{4}$ in. and that of the thick part was 3 in. The thin part was intended for $|t| < 0.4$ $(\mathrm{GeV}/c)^2$, where the protons had shorter range, while the thick part was to increase rates at $0.4 < |t| < 1.0$ $(\mathrm{GeV}/c)^2$.

The polarimeter was oriented so that its normal made an angle of 55.5° with respect to the beam line. This was done so that most of the recoil protons would enter normal to the carbon. The magnetic field of the PPT magnet was such that there was only a small variation in the angle at which the protons entered the carbon (see Table II). Typical trajectories are shown in Fig. 2, and

TABLE II. The kinematical quantities for pp elastic scattering at several t values and $P_{lab} = 6$ GeV/c.

$\|t\|$ [(GeV/c)^2]	$\theta_{c.m.}$ (deg)	θ_R (deg)	P_R (MeV/c)	T_R (MeV)	θ_{rot} (deg)	θ_{net} (deg)
0.27	19.2	72.0	535	140	16.1	55.9
0.38	23.0	68.5	650	205	13.2	55.4
0.51	26.7	65.4	756	275	11.2	54.2
0.66	30.4	62.3	890	350	9.7	52.6
0.83	34.1	59.4	1010	440	8.5	50.9
1.00	37.7	56.6	1135	535	7.6	49.1

$$\theta_{rot} = \frac{3\times10^{-4}\int B\cdot dl}{P_R} = \frac{150}{P_R\,(\mathrm{MeV}/c)}, \quad \theta_{net} = \theta_R - \theta_{rot}$$

the distribution of incident angles observed at the carbon plate is shown in Fig. 3. The polarimeter had 360° azimuthal acceptance. The $\hat{N}$ component of the recoil spin was measured by a left-right asymmetry and the $\hat{S}$ component by an up-down asymmetry of the scattered particles by the carbon analyzer.

In Fig. 4, the average momentum (kinetic energy) expected of recoil protons at the center of $\frac{3}{4}$- and 3-in.-thick carbon plates is shown as a function of t, the momentum transfer square of the primary scattering. The limit to the angular resolution comes mostly from the multiple scattering through the carbon plates as shown in Fig. 5, while the intrinsic resolution expected due to finite wire spacing is 0.87°.

IV. DATA ANALYSIS AND RESULTS

The data analysis consisted of three stages: filter, single-scattering, and polarimeter analysis. At the filter stage, obviously bad events were removed, such as the ones containing no hits in the forward and/or the recoil chambers, or the ones with too many hits in a chamber. Typically, 80% of the events were transmitted to high-density tape for further analysis. At the stage of single-scattering, kinematical quantities were calculated for the events which had one and only one track in each of the beam, forward, and recoil arms. In a few percent of these events, the recoil protons scattered in the carbon plate, and the information of those with large enough scattering angles ($\theta > 4°$) were written out for the polarimeter analysis. The polarimeter analysis cut and divided these

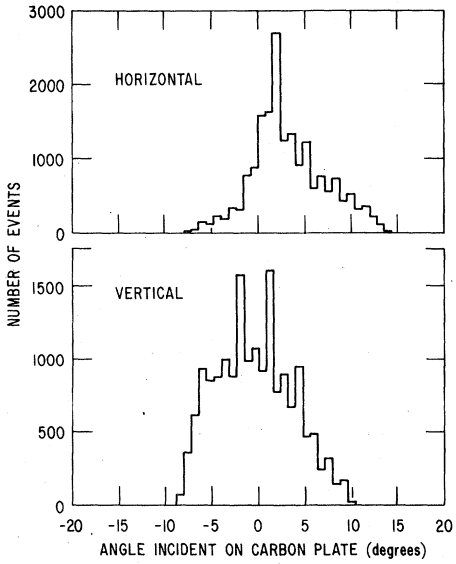

FIG. 3. Distribution of incident angles at the carbon plate.

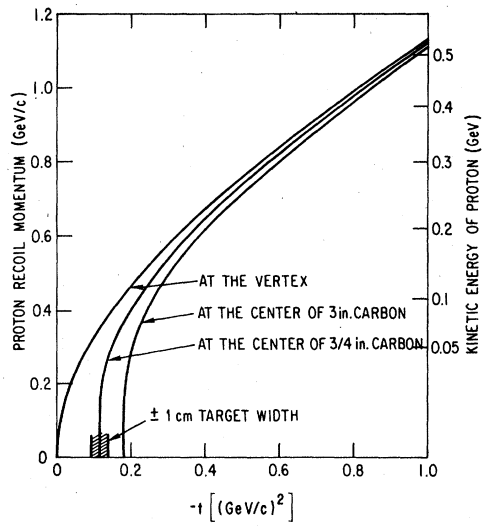

FIG. 4. Proton momentum expected at the center of carbon plate as a function of t, the momentum transfer squared of the primary scattering.

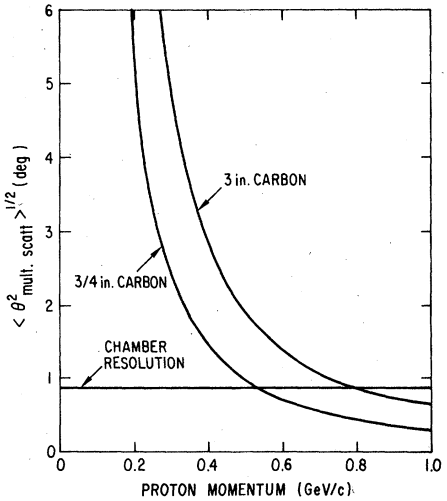

FIG. 5. The multiple-scattering angle $\langle\theta^2\rangle^{1/2}$ vs proton momentum through $\frac{3}{4}$ or 3-in. carbon plates.

events into bins of azimuthal angle of the scattering at the carbon plate. The double- and triple-spin correlation parameters were calculated by obtaining the left-right or up-down asymmetry for each combination of the beam and the target polarization. About 3×10^7 events were logged on tape, and the final sample of about 3×10^4 events survived cuts and were used to obtain the double-scattering parameters. More detailed descriptions of the last two stages of analysis are given below.

A. Single-scattering analysis and its results

Besides the desired elastic-scattering events, two kinds of background were present, inelastic and quasielastic scattering. The latter is the scattering from bound protons in the complex nuclei present in the target. Elastically scattered events satisfy two conditions, a forward-recoil angle correlation and a coplanarity condition, where the beam, scattered, and recoil protons were in a plane. An event was called coplanar if its coplanarity angle was within some limit, typically 6°. Elastic scattering events would show up as a sharp peak over a much broader background when the coplanar events were plotted vs the recoil angle for a given bin of the forward scattering angle. The number of elastic events was then obtained by subtracting the background under the peak. The method of this subtraction is described in detail in Ref. 9. When the beam is polarized in the $\vec{S}$ direction, and the target in the $\vec{N}$ direction, the differential cross section in each t bin is given by

$$I_1^{\pm\pm}=I_0\{1\pm P_B I_n(S,0;0,0)\pm P_T I_n(0,N;0,0) + (\pm P_B)(\pm P_T)C_{SN}\},$$

where I_0 is the spin-averaged cross section, and $(\pm P_B)$ and $(\pm P_T)$ refer to the beam and target polarization. We obtain the parameters by inverting a 4×4 matrix:

$$\begin{pmatrix} I_1^{++} \\ I_1^{-+} \\ I_1^{+-} \\ I_1^{--} \end{pmatrix} = \begin{pmatrix} 1 & +P_B & +P_T & +P_BP_T \\ 1 & -P_B & +P_T & -P_BP_T \\ 1 & +P_B & -P_T & -P_BP_T \\ 1 & -P_B & -P_T & +P_BP_T \end{pmatrix} \times \begin{pmatrix} I_0 \\ I_0 I_n(S,0;0,0) \\ I_0 I_n(0,N;0,0) \\ I_0 C_{SN} \end{pmatrix},$$

or in matrix form

$$R_1=\sum_j M_{ij}O_j .$$

Then the solution is

$$O_1=\sum_j (M^{-1})_{ij}R_j .$$

The results are given in Fig. 6. The parameters $I_n(S,0;0,0)$ and C_{SN} are expected to be equal to zero by parity conservation, and the experimental verification of this shows that the systematic errors are under control. The parameter $I_n(0,N;0,0)$ is the polarization parameter, and it agrees well with earlier published results.[5-9,11]

B. Polarimeter analysis

It is very important to have a good alignment of the four MWPC's in the polarimeter. The positions were carefully surveyed at the time of setting up, and a slight adjustment was made by analyzing the data taken with no carbon plate. A scattering in the carbon was determined by the following criteria: (a) The two straight lines determined by the first two (and the last two) polarimeter planes must have a distance of minimum approach < 0.5 cm, (b) the midpoint of the closest approach was assumed to be the location of the second scattering and must be within the carbon, and (c) the angle of the second scattering must be in the range from 6° to 16° (see Appendix A for this choice). In addition, the same cuts were

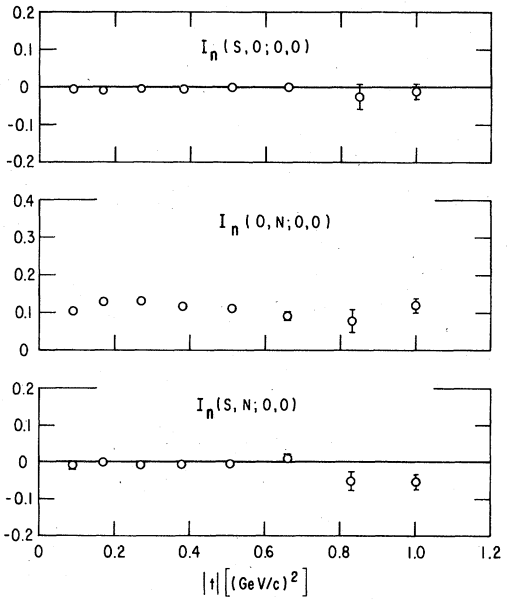

FIG. 6. The results for single-scattering parameters $\tilde{I}_n(S,0;0,0)$ $I_n(0,N;0,0)=P$ and $\tilde{C}_{SN}$. The first and the last quantities should vanish under the parity invariance, while the second one is the polarization parameter.

applied to the first scattering quantities as for the single-scattering analysis. Note that in this sample, the background events under the elastic peak are inevitably included. The differential cross section for the double scattering of this experiment at fixed t is given by

$$
\begin{aligned}
I_2^{\pm\pm} = I_0[1 + B \pm P_B \tilde{I}_n(S,0;0,0) \pm P_T I_n(0,N;0,0) + (\pm P_B)(\pm P_T)\tilde{C}_{SN}] \\
- I_0 \bar{A}[I_n(0,0;0,N) \pm P_B \tilde{K}_{SN} \pm P_T D_{NN} + (\pm P_B)(\pm P_T)\tilde{H}_{SNN}] \cos\phi \\
+ I_0 \bar{A}[I_n(0,0;0,S) \pm P_B \tilde{K}_{SS} \pm P_T D_{NS} + (\pm P_B)(\pm P_T)\tilde{H}_{SNS}] \sin\phi ,
\end{aligned}
$$

where $\bar{A}$ is the analyzing power of carbon, and ϕ is the azimuthal scattering angle of the second scattering measured from the primary scattering plane at the carbon. The quantity B is the ratio of the number of background events under the elastic peak to that of elastic events, and is obtained after the polarimeter cuts were applied. We assumed that the background events do not carry any spin information, which was experimentally checked within the statistical accuracy by analyzing noncoplanar events in the same way. The reason for the tildes on some of the parameters is that the magnetic field of the PPT precessed the spins of incident and recoil protons and mixed in other parameters as described in Sec. IV D.

The events were grouped into 24 angular bins in ϕ, accumulated, and then projected onto the four directions: left, right, up, and down. Only the bins within $\pm 67.5^\circ$ about each direction were combined, which is the optimum as shown in Appendix A. The projection to left or right, up or down yields

$$
\begin{pmatrix} I_L^{++} \\ I_R^{++} \\ I_L^{-+} \\ I_R^{-+} \\ I_L^{+-} \\ I_R^{+-} \\ I_L^{--} \\ I_R^{--} \end{pmatrix} = MI_0 \begin{pmatrix} 1+B \\ I_n(S,0;0,0) \\ I_n(0,N;0,0) \\ C_{SN} \\ I_n(0,0;0,N) \\ \tilde{K}_{SN} \\ D_{NN} \\ \tilde{H}_{SNN} \end{pmatrix} \text{ and } \begin{pmatrix} I_D^{++} \\ I_U^{++} \\ I_D^{-+} \\ I_U^{-+} \\ I_D^{+-} \\ I_U^{+-} \\ I_D^{--} \\ I_U^{--} \end{pmatrix} = MI_0 \begin{pmatrix} 1+B \\ \tilde{I}_n(S,0;0,0) \\ I_n(0,N;0,0) \\ \tilde{C}_{SN} \\ \tilde{I}_n(0,0;0,S) \\ \tilde{K}_{SS} \\ \tilde{D}_{NS} \\ \tilde{H}_{SNS} \end{pmatrix} ,
$$

where

$$
M = \begin{Bmatrix}
1+B & P_B & P_T & P_BP_T & \bar{A} & \bar{A}P_B & \bar{A}P_T & \bar{A}P_BP_T \\
1+B & P_B & P_T & P_BP_T & -\bar{A} & -\bar{A}P_B & -\bar{A}P_T & -\bar{A}P_BP_T \\
1+B & -P_B & P_T & -P_BP_T & \bar{A} & -\bar{A}P_B & \bar{A}P_T & -\bar{A}P_BP_T \\
1+B & -P_B & P_T & -P_BP_T & -\bar{A} & \bar{A}P_B & -\bar{A}P_T & \bar{A}P_BP_T \\
1+B & P_B & -P_T & -P_BP_T & \bar{A} & \bar{A}P_B & -\bar{A}P_T & -\bar{A}P_BP_T \\
1+B & P_B & -P_T & -P_BP_T & -\bar{A} & -\bar{A}P_B & \bar{A}P_T & \bar{A}P_BP_T \\
1+B & -P_B & -P_T & P_BP_T & \bar{A} & -\bar{A}P_B & -\bar{A}P_T & \bar{A}P_BP_T \\
1+B & -P_B & -P_T & P_BP_T & -\bar{A} & \bar{A}P_B & AP_T & -\bar{A}P_BP_T
\end{Bmatrix}
$$

and $\bar{A} = fA$, where $f = 0.826$ is the reduction of the analyzing power due to the use of a wider azimuthal range (see Appendix A).

In matrix form

$$R_i = \sum_j M_{ij} O_j ,$$

and the solution is

$$O_i = \sum_j (M^{-1})_{ij} R_j .$$

C. Determination of analyzing power

Looking at the equations above for left-right, we see that one of the experimentally measured asymmetries is

$$\epsilon = fAP_T D_{NN} .$$

A can be obtained by using values of D_{NN} measured in other experiments (see Fig. 7). As the experimental values are not accurate enough, we have

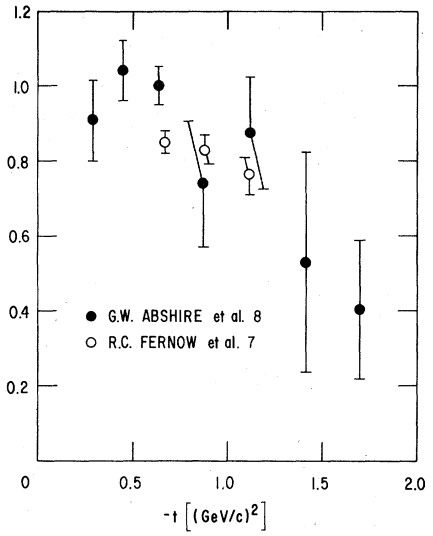

FIG. 7. D_{NN} vs $-t$ for $P_{\text{lab}} = 6$ GeV/c (data from Refs. 7 and 8).

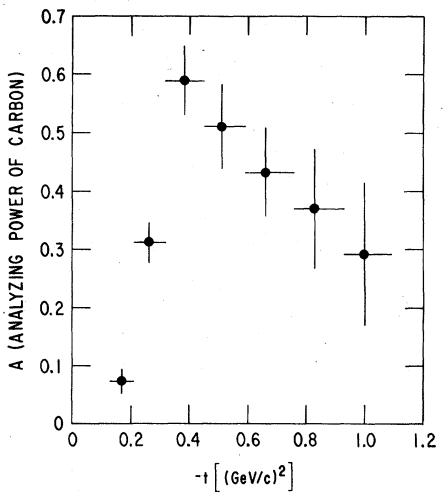

FIG. 8. The values of the analyzing power $A(t)$ as a function of t obtained by assuming $D_{NN}(t) = 0.95$.

assumed $D_{NN} = 0.95$ over our complete t range. The resulting analyzing power is shown in Fig. 8. These values are in generally good agreement with the ones reported in the literature.[12]

Note that we need to divide by A, the analyzing power, to obtain double-scattering quantities, and its uncertainty causes an overall normalization error, which we do not include in the final results in this paper. We intend to calibrate the polarimeter using the polarized beams at Argonne ZGS, and the final results will be rescaled accordingly if found necessary.

D. Corrections due to the magnetic field

The magnetic field of the PPT magnet precessed the spin of the incoming proton in the horizontal plane by about $14.6°$; i.e., the beam polarization was given by $(0.251\vec{L} + 0.968\vec{S})P_B$. Thus,

$$\tilde{I}_n(S,*;*,*) = 0.251 I_n(L,*;*,*) + 0.968 I_n(S,*;*,*),$$

where $*$ indicates any spin direction of O, N, L, and S.

Similarly, the spin of the recoil protons was also precessed, causing the polarimeter to analyze a mixture of $\vec{L}$ and $\vec{S}$ rather than pure $\vec{S}$, for the case of up-down asymmetry. The amount of the precession is dependent on t. The explicit expressions for the amount of mixtures are given in Table III for $\tilde{K}_{SS}$ and $\tilde{H}_{SNS}$. These values were calculated by tracing protons of various kinematical values through the PPT magnetic field.

E. Results of the double scattering

The results are given in Fig. 9 and Table IV. The errors shown are statistical only, and the errors due to the analyzing power are not folded in. The latter should be understood as an overall normalization uncertainty of $\pm \Delta A/A$, where A is the analyzing power of the carbon.

Parameters $\tilde{K}_{SN}$, $\tilde{H}_{SNN}$, $\tilde{I}_n(0,0;0,S)$, and $\tilde{D}_{NS}$ are expected to vanish owing to parity conservation. The parameter $I_n(0,0;0,N)$ is the polarization parameter, and it must agree with the single-scattering parameter $I_n(0,N;0,0)$. The results shown in

TABLE III. The amount of mixture of observables $\tilde{K}_{SS}$ and $\tilde{H}_{SS}$ due to the PPT magnetic field.

$\tilde{K}_{SS} = \alpha K_{LL} + \beta K_{SL} + \gamma K_{LS} + \delta K_{SS}$

$-t$ [(GeV/c)^2]	α	β	γ	δ
0.27	−0.16	0.61	−0.19	0.75
0.38	−0.13	0.49	−0.22	0.84
0.51	−0.11	0.43	−0.23	0.87
0.66	−0.10	0.39	−0.23	0.89
0.83	−0.09	0.36	−0.23	0.90
1.00	−0.09	0.34	−0.23	0.90

$\tilde{H}_{SNS} = \alpha H_{LNL} + \beta H_{SNL} + \gamma H_{LNS} + \delta H_{SNS}$

$-t$ [(GeV/c)^2]	α	β	γ	δ
0.27	−0.16	0.61	−0.19	0.75
0.38	−0.13	0.49	−0.22	0.84
0.51	−0.11	0.43	−0.23	0.87
0.66	−0.10	0.39	−0.23	0.89
0.83	−0.09	0.36	−0.23	0.90
1.00	−0.09	0.34	−0.23	0.90

Fig. 9 are in fair agreement with these expectations. Deviations from an expectation indicates a presence of biases. Effects of various biases are studied in some detail in Appendix B. We conclude that the desired parameters $\tilde{K}_{SS}$ and $\tilde{H}_{SNS}$ are little affected within the accuracy of the present measurement.

F. Discussion of results

1. $\tilde{H}_{SNS}$

The results shown in Fig. 9 indicate that $\tilde{H}_{SNS} = 0.098 \pm 0.085$ over the $|t|$ range measured, with rather large statistical errors. Without waiting for the full amplitude analysis, we would like to study the implications in a crude way here to convey to the readers some feeling of what we learn from these results. We ignore for a moment the complication of the mixing of other components and use rather simplified arguments.

The parameter H_{SNS} can be approximately expressed as the following according to Table I:

$$H_{SNS} \simeq 2\,\mathrm{Im}(N_0 U_2^*)/I_0 \simeq 2U_{2\perp}/|N_0|$$

or $U_{2\perp}|N_0| \sim 0.05 \pm 0.04$ from our measurement. Here we assume that the amplitude N_0 is dominant over the others[4] and $U_{2\perp}$ is the orthogonal component of U_2 relative to N_0. The other component $U_{2\parallel}|N_0|$ is determined to be about -0.05 from the measurement of the parameter C_{SS}.[10] Knowing $\mathrm{Re}N_0/\mathrm{Im}N_0 \simeq -0.3$ at $t \sim 0$,[13] and assuming its slow dependence on t, one finds that the U_2 amplitude is consistent with being real and positive as shown in Fig. 10. At high energy, the amplitude U_2 corresponds to $\pi(B)$ exchange, and the observed values are consistent with the expectation for the amplitude.[14] The actual amplitude determination will be done rigorously, taking the mixing into account and without assuming the N_0 dominance.

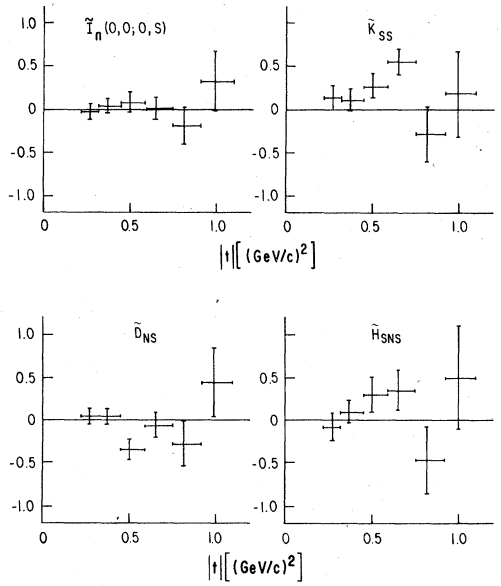

FIG. 9. The results of double-scattering parameters plotted vs $-t$.

2. $\tilde{K}_{SS}$

Under the assumption of N_0 dominance, we expect the following relation to hold (see Table I):

TABLE IV. The results of the double-scattering analysis. [a]

Left-right						
$-\bar{t}$ $[(\mathrm{GeV}/c)^2]$	$-t_{\min}$ $[(\mathrm{GeV}/c)^2]$	$-t_{\max}$ $[(\mathrm{GeV}/c)^2]$	$I_n(0,0;0,N)$	$\tilde{K}_{SN}$	$\tilde{D}_{NN}$	$\tilde{H}_{SNN}$
0.27	0.22	0.32	0.24 ± 0.09	0.01 ± 0.13	0.95 ± 0.11	-0.24 ± 0.16
0.37	0.32	0.45	0.08 ± 0.08	0.08 ± 0.12	0.95 ± 0.10	0.02 ± 0.14
0.50	0.45	0.59	0.23 ± 0.11	-0.04 ± 0.16	0.95 ± 0.13	0.26 ± 0.19
0.65	0.59	0.75	0.34 ± 0.13	-0.15 ± 0.20	0.95 ± 0.16	0.12 ± 0.24
0.81	0.75	0.92	0.00 ± 0.21	0.10 ± 0.32	0.95 ± 0.26	-0.04 ± 0.38
0.99	0.92	1.10	0.28 ± 0.33	-0.11 ± 0.49	0.95 ± 0.40	-0.21 ± 0.59
Up-down						
$-\bar{t}$ $[(\mathrm{GeV}/c)^2]$	$-t_{\min}$ $[(\mathrm{GeV}/c)^2]$	$-t_{\max}$ $[(\mathrm{GeV}/c)^2]$	$I_n(0,0;0,S)$	$\tilde{K}_{SS}$	$\tilde{D}_{NS}$	$\tilde{H}_{SNS}$
0.27	0.22	0.32	-0.03 ± 0.09	0.14 ± 0.14	0.05 ± 0.11	-0.07 ± 0.16
0.37	0.32	0.45	0.04 ± 0.08	0.11 ± 0.12	0.05 ± 0.10	0.10 ± 0.14
0.50	0.45	0.59	0.08 ± 0.11	0.26 ± 0.16	-0.34 ± 0.13	0.30 ± 0.20
0.65	0.59	0.75	0.01 ± 0.13	0.67 ± 0.20	-0.06 ± 0.16	0.35 ± 0.24
0.81	0.75	0.92	-0.19 ± 0.22	-0.27 ± 0.33	-0.27 ± 0.26	-0.45 ± 0.39
0.99	0.92	1.10	0.32 ± 0.34	0.19 ± 0.50	0.44 ± 0.40	0.49 ± 0.61

[a] The analyzing power was determined to make $D_{NN} = 0.95$.

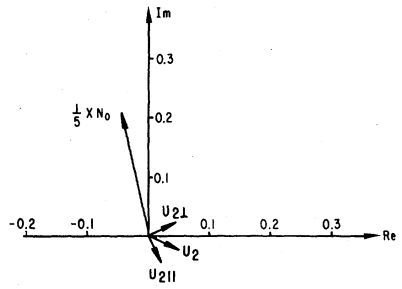

FIG. 10. The amplitudes N_0 and U_2 (corresponding to π exchange) at small t at 6 GeV/c in an Argand diagram.

$$K_{SS} \simeq 2\,\mathrm{Re}(N_0 U_2^*)\cos\theta_R/I_0$$
$$\simeq -C_{SS}\cos\theta_R \simeq +0.1\cos\theta_R\,.$$

Data point lie above this naive expectation with large error bars. But, we note that K_{SS} contains other parameters, notably K_{SL} as seen in Table IV, which is given approximately as

$$K_{SL} \simeq -2\,\mathrm{Re}(N_0 U_2^*)\sin\theta_R/I_0$$
$$\simeq -C_{SS}\sin\theta_R \simeq +0.1\sin\theta_R\,,$$

and the observed values are consistent by including this effect.

3. *Concluding remarks*

Even though double- and triple-spin correlation measurements have become much easier by using a polarized beam and target, the error bars shown in Fig. 9 are still fairly large. This is because very few recoil protons scatter in the carbon polarimeter plate with a large enough angle to have a nonzero analyzing power. Given a reasonable running time, it is necessary to increase the beam intensity and at the same time to suppress those events that do not have a large enough scattering angle in the carbon plate. Recently, we have incorporated such a hardware device, which has made it possible to increase the beam intensity by at least a factor of 4.

ACKNOWLEDGMENTS

We are grateful to Dr. S. T. Wang and F. Onesto for designing and bringing the superconducting solenoid into operation, to R. C. Miller for his help in analysis and polarized-target preparation, and to R. Daly and W. Haberichter for their help with the multiwire-proportional-chamber system. We also wish to thank O. Fletcher, T. Kasprzyk, E. Millar, and A. Rask for their help in setting up and running this experiment, and Dr. N. Tamura for his help in the polarimeter analysis. This work was supported by the U. S. Department of Energy.

APPENDIX A: OPTIMIZATION OF POLARIMETER θ-φ APERTURE

The angular distribution of protons scattering on carbon (a spin-0 nucleus) can be written as

$$N(\theta,\varphi) \propto \sigma_0(\theta)[1 - PA(\theta)\sin(\varphi - \varphi_0)]$$
$$= \sigma_0(\theta)[1 + A(\theta)(\alpha\cos\varphi + \beta\sin\varphi)]\,, \quad \text{(A1)}$$

where $\sigma_0(\theta)$ is the spin-averaged scattering cross section, θ is the polar scattering angle, P is the net polarization of the protons, φ is the scattering azimuthal angle measured relative to the primary scattering plane of the proton, and φ_0 is the azimuthal angle of the proton's polarization vector relative to the same plane. α and β are more closely related to the observables we wish to measure.

If we consider left-right scattering, we wish to find the aperature $\theta_1 < \theta < \theta_2$, $|\varphi| < \varphi_1$ such that the statistical error on α is minimized. (The terms in $\beta\sin\varphi$ are canceled out by averaging over this φ region.) The number of events to the left (N_L) and right (N_R) are proportional to

$$N_L = \int_{\theta_1}^{\theta_2}\sigma_0(\theta)\int_{-\varphi_1}^{\varphi_1}[1 + \alpha A(\theta)\cos\varphi]d\theta\,d\varphi$$
$$= 2\langle\sigma_0\rangle\varphi_1(1 + \alpha\langle A\rangle\sin\varphi_1/\varphi_1)\,,$$
$$N_R = 2\langle\sigma_0\rangle\varphi_1(1 - \alpha\langle A\rangle\sin\varphi_1/\varphi_1)\,, \quad \text{(A2)}$$

where

$$\langle\sigma_0\rangle = \int_{\theta_1}^{\theta_2}\sigma_0(\theta)d\theta\,,$$
$$\langle A\rangle = \int_{\theta_1}^{\theta_2}\sigma_0(\theta)A(\theta)d\theta/\langle\sigma_0\rangle\,.$$

The measured asymmetry is

$$\epsilon = (N_L - N_R)/(N_L + N_R)$$
$$= \alpha\langle A\rangle\sin\varphi_1/\varphi_1\,, \quad \text{(A3)}$$

and the desired result is

$$\alpha = \frac{\epsilon}{\langle A\rangle}\frac{\varphi_1}{\sin\varphi_1}\,.$$

The statistical error on α is given as follows:

$$\Delta = \frac{1}{\langle A\rangle}\frac{\varphi_1}{\sin\varphi_1}\left(\frac{1-\epsilon^2}{N_L + N_R}\right)^{1/2}\,.$$

This can be rewritten using (A2) as

$$\Delta^{-1} = 2(1-\epsilon^2)^{-1/2}(\sin^2\varphi_1/\varphi_1)^{1/2}(\langle A\rangle^2\langle\sigma_0\rangle)^{1/2}\,. \quad \text{(A4)}$$

Δ can be minimized easily if we assume that $\epsilon \ll 1$. In this case the problem decouples and $\sin^2\varphi_1/\varphi_1$ and $\langle A\rangle^2\langle\sigma_0\rangle$ can be maximized independently.

1. φ aperture

$\sin^2\varphi_1/\varphi_1$ is maximized by solving $\tan\varphi_1 = 2\varphi_1$. The solution is 0.72 at $\varphi_1 = 66.78°$. At this value of φ_1, the effective analyzing power is $f\langle A\rangle$, where $f = \sin\varphi_1/\varphi_1 = 0.78$. (In the data analysis, the data are binned in 15° bins and φ_1 is taken as 60°, so $f = 0.826$.)

2. θ aperture

$y = \langle A^2\rangle\langle\sigma_0\rangle$ is maximized with respect to θ_1 and θ_2 by plotting y on a (θ_1, θ_2) grid and finding the peak. As an example, proton-carbon elastic scattering data[15] at 313 MeV give $y_{max} \sim 850$ mb/sr at $(\theta_1, \theta_2) = (4°, 16.2°)$. We have chosen $\theta_1 = 6°$ to avoid contributions from multiple Coulomb scattering, and $\theta_2 = 16°$ to ensure that all scattered protons are within the aperture of the MWPC's. $y \sim 620$ mb/sr at (6°, 16°) and the increase in Δ is $(850/620)^{1/2} = 1.17$. We ignore effects associated with inelastic proton-carbon scattering for this calculation.

APPENDIX B: EFFECT OF BIASES TO THE DOUBLE-SCATTERING OBSERVABLES

1. Inefficiency in the polarimeter chambers

The largest possible bias present in our system is the inefficiency in the various regions of the polarimeter chambers. In order to study this problem, the equation in Sec. VIB is written as $R_{obs} = I_0 M C_{obs}$. To include the effect of inefficiency we must multiply alternate rows of the right-hand side by ϵ_a and ϵ_b [right (down) and left (up) efficiencies]. Defining

$$\epsilon = \tfrac{1}{2}(\epsilon_a + \epsilon_b) \quad \text{and} \quad \Delta = (\epsilon_a - \epsilon_b)/(\epsilon_a + \epsilon_b),$$

we can absorb ϵ (average efficiency) into I_0 and define $D_{ij} = (-1)^i \delta_{ij}$. Then the modified equation is

$$R_{obs} = I_0(I + \Delta D)MC,$$

where $I_{ij} = \delta_{ij}$, so

$$I_0 M C_{obs} = I_0(I + \Delta D)MC,$$

$$C_{obs} = M^{-1}(I + \Delta D)MC$$

$$= (I + \Delta M^{-1} D M)C.$$

Now we can show that owing to the symmetry of M (assuming $A_a = A_b$), $DM = MP$, where P is a permutation matrix

$$\begin{pmatrix} 0 & A \times I \\ I/A & 0 \end{pmatrix}$$

(shown in submatrix format). Then

$$C_{obs} = (I + \Delta M^{-1} M P)C$$

$$= (I + \Delta P)C.$$

The result of this exercise is to demonstrate that the calculated observables (C_{obs}) can be mixtures of the desired ones if the efficiencies are not equal. The mixtures are simply between observables where the polarimeter is (or is not) used.

(a) $I_n(0,0;0,K)$ is mixed with $I_n(0,0;0,0)$ as $I_n(0,0;0,K) + (\Delta/A) I_n(0,0;0,0)$. That is, an asymmetry is introduced of size Δ/A. We assume that $I_n(0,0;0,S)$ is equal to zero and any observed effects are due to unequal efficiencies.

(b) $K_{Sk} \to K_{Sk} + (\Delta/A) I_n(S,0;0,0)$ should have no bias.

(c) $D_{Nk} \to D_{Nk} + (\Delta/A) I_n(0,N;0,0)$. D_{NS} could show a bias ~0.1 times that of $I_n(0,0;0,S)$. D_{NN} could have a bias which affects the analyzing power.

(d) $H_{SNk} \to H_{SNk} + (\Delta/A) I_n(S,N;0,0)$ should have no bias.

(e) The single-scattering results are mixed with double-scattering parameters multiplied by $\Delta \times A$. These effects are too small to be observed.

2. Difference in analyzing power

Varying efficiency over the polarimeter chambers or misalignment of chambers implies that the analyzing power could also be different, when the latter is not constant over the accepted angular range of 6° to 16°. An analysis similar to the one for efficiency differences shows that $C_{obs} = (I + \Delta_A P_A)C$, where Δ_A is the asymmetry in the analyzing powers $(A_a - A_b)/(A_a + A_b)$ and P_A is a matrix

$$\begin{pmatrix} 0 & A \times I \\ 0 & 0 \end{pmatrix}.$$

This means that the double-scattering observables are not affected, but the single-scattering observables are affected by the double-scattering ones, which is a negligible effect, except for $I_n(0,N;0,0)$, which will contain effects due to $D_{NN} = I_n(0,N;0,N)$.

3. Misalignment of chambers

This effect is essentially the same as the case for inefficiencies.

---

*Present address: Fermi National Accelerator Laboratory, Batavia, Ill.

†Present address: General Electric Co., Milwaukee, Wis.

‡Present address: University of Tokyo, Hongo, Bunkyo-ku, Japan.

[1]See, e.g., R. A. Arndt *et al.*, Phys. Rev. 182, 1714 (1969).

[2]C. R. Shumacher and H. A. Bethe, Phys. Rev. 121, 1534 (1961).
[3]F. Halzen and G. H. Thomas, Phys. Rev. D 10, 344 (1974).
[4]P. W. Johnson, R. C. Miller, and G. H. Thomas, Phys. Rev. D 15, 1895 (1977).
[5]M. Borghini *et al.*, Phys. Lett. 31B, 405 (1970) (P).
[6]D. R. Rust *et al.*, Phys. Lett. 58B, 114 (1975) (P).
[7]R. C. Fernow *et al.*, Phys. Lett. 52B, 243 (1974) (P, C_{NN},D_{NN},K_{NN}); also see T. A. Mulera, in *High Energy with Polarized Beams and Targets*, proceedings of the Argonne Symposium, 1976, edited by M. L. Marshak (AIP, New York, 1976) [AIP Conf. Proc. 35, 83 (1976)].
[8]G. W. Abshire *et al.*, Phys. Rev. D 12, 3393 (1975) (D_{NN}).
[9]D. Miller *et al.*, Phys. Rev. Lett. 36, 763 (1976); Phys. Rev. D 16, 2016 (1977) (P,C_{NN}).
[10]I. P. Auer *et al.*, Phys. Rev. Lett. 37, 1727 (1976) (C_{SS}); Phys. Lett. 70B, 475 (1977) (C_{LL}).
[11]J. Deregel *et al.*, Nucl. Phys. B103, 269 (1976) (P,R).
[12]See, e.g., D. Besset *et al.*, Nucl. Instrum. Methods 148, 129 (1978).
[13]U. Amaldi, M. Jacob, and G. Matthiae, Annu. Rev. Nucl. Sci. 26, 385 (1976).
[14]G. L. Kane, in *High Energy Physics with Polarized Beams and Targets* (Ref. 7), p. 43.
[15]O. Chamberlain *et al.*, Phys. Rev. 102, 1659 (1956).